

Finite Element Lattice Boltzmann Simulations of Contact Line Dynamics

Rastin Matin,^{*} Marek Krzysztof Misztal,[†] Anier Hernández-García, and Joachim Mathiesen
Niels Bohr Institute, University of Copenhagen, DK-2100 Copenhagen, Denmark

(Dated: April 18, 2022)

The lattice Boltzmann method has become a standard technique for simulating a wide range of fluid flows. However, the intrinsic coupling of momentum and space discretization restricts the traditional lattice Boltzmann method to regular lattices. Alternative off-lattice Boltzmann schemes exist for both single- and multiphase flows that decouple the velocity discretization from the underlying spatial grid. The current study extends the applicability of these off-lattice methods by introducing a finite element formulation that enables simulating contact line dynamics for partially wetting fluids. This work exemplifies the implementation of the scheme and furthermore presents benchmark experiments that show the scheme reduces spurious currents at the liquid-vapor interface by two orders of magnitude compared to a nodal implementation and allows for predicting the equilibrium states accurately in the range of moderate contact angles.

PACS numbers: 47.11.-j, 47.55.dr, 47.60.+i

I. INTRODUCTION

The interaction between a liquid and a solid surface plays an important role in many fields ranging in scale from below those considered in microfluidics to scales beyond those in reservoir modelling. In this context the static contact angle defines the intersection between a liquid-vapor interface and a solid surface and specifies the degree of wettability of the surface through Young's equation.

The lattice Boltzmann method (LBM) is a popular method within computational fluid dynamics and several regular-grid based multiphase formulations have emerged within the last 15 years that successfully describe fluid-solid interactions, thereby enabling the simulation of wetting effects. These formulations fall within different categories such as free-energy ([1–7]) and interparticle-potential ([8–10]) schemes and have been used, for example, in studies of droplet spreading (*e.g.* [7, 10–12]) and fluid flow in porous media (*e.g.* [13–19]). In particular free-energy based LBMs have become a useful tool for the study of wetting phenomena [20]. One of the main advantages of these models over other variants such as interparticle potential (Shan-Chen) is that the surface tension is more easily tuned and the kinematic viscosity ratio and density ratio can be chosen independently [20]. Free-energy based LBMs enforce the wetting boundary condition on the wall implicitly in the intermolecular force. On regular grids this is accomplished by specifying the terms in the finite-difference derivatives at the solid boundary [5–7, 21].

A different class of LBM exists generally known as off-lattice Boltzmann methods, where the spatial and temporal discretizations are decoupled for enhanced geometric flexibility. This class consists of finite volume [22–24] and finite element schemes [25–30]. However, previ-

ous work on multiphase finite element LBM (FE-LBM) has only regarded the intermolecular force term [29, 30] and liquid-solid interactions have not been accounted for. In this paper we present an extension of our previous characteristic-based FE-LBM scheme [30] by implementing wetting boundary conditions and moving the intermolecular force term to the streaming step. Our formulation is shown to further reduce spurious currents at equilibrium compared to the implementation in [30]. To the best of our knowledge, this is the first formulation of wetting boundaries in the framework of off-lattice Boltzmann methods.

The paper is organized as follows: In Section II the multiphase model and wall boundary conditions are briefly reviewed. This section also details the FE-LBM on unstructured grids. The scheme is validated in Section III and results are summarized in Section IV.

II. NUMERICAL METHOD

We consider the diffuse interface model for incompressible immiscible two-phase flows with large density and kinematic viscosity ratios presented in [6, 7, 29]. The main aspects of the model are briefly summarized in the following to provide context.

The composition $C \in [0, 1]$ is chosen as the volume fraction of the liquid phase, *i.e.*, $C = 1$ for the liquid (l) phase and $C = 0$ for the vapor (v) phase. The time evolution of the diffuse interface is governed by a Cahn-Hilliard equation

$$\partial_t C + \mathbf{u} \cdot \nabla C = M \nabla^2 \mu, \quad (1)$$

where $M > 0$ is the mobility. The chemical potential μ in Eq. (1) follows from the free-energy functional

$$\Psi_b = \int_V \left(\beta C^2 (1 - C)^2 + \frac{\kappa}{2} |\nabla C|^2 \right) dV, \quad (2)$$

where $E_0(C) = \beta C^2 (1 - C)^2$ is the bulk free energy density. Here β and κ are constants related to the surface

^{*} rastin@nbi.ku.dk

[†] misztal@nbi.ku.dk

tension and interface width. From thermodynamics it follows that

$$\mu = \frac{\delta\Psi_b}{\delta C} = 2\beta C(C-1)(2C-1) - \kappa\nabla^2 C \quad (3)$$

and the plane interfacial profile in equilibrium follows from setting $\mu = 0$,

$$C(z) = \frac{1}{2} + \frac{1}{2} \tanh\left(\frac{2z}{\xi}\right). \quad (4)$$

Here z is the coordinate normal to the interface, $\xi = \sqrt{8\kappa/\beta}$ the interface thickness and $\sigma = \sqrt{2\kappa\beta}/6$ its surface tension. Disregarding body forces, the governing macroscopic equations for the incompressible flow are

$$\nabla \cdot \mathbf{u} = 0 \quad (5)$$

$$\rho\left(\partial_t \mathbf{u} + \mathbf{u} \cdot \nabla \mathbf{u}\right) = -\nabla p - C\nabla\mu \quad (6)$$

$$+ \nabla \cdot [\eta(\nabla \mathbf{u} + (\nabla \mathbf{u})^T)]$$

where p is the hydrodynamic pressure, η the dynamic viscosity and $\rho = C\rho_l + (1-C)\rho_v$ the density.

A. Lattice Boltzmann Method

Recovering the Cahn-Hilliard, pressure evolution and momentum equations in a lattice Boltzmann framework can be accomplished by introducing two particle distribution functions g_α and h_α . The distribution function h_α recovers the composition that tracks the interface between the two phases and g_α recovers the hydrodynamic flow fields. The lattice Boltzmann equation for each distribution function is given by [6, 29]

$$\partial_t g_\alpha + e_{\alpha i} \partial_i g_\alpha = -\Omega_{g_\alpha} + F_{g_\alpha} \quad (7)$$

$$\partial_t h_\alpha + e_{\alpha i} \partial_i h_\alpha = -\Omega_{h_\alpha} + F_{h_\alpha} \quad (8)$$

where the intermolecular forcing term F_{ψ_α} and BGK-operator Ω_{ψ_α} for a given distribution function $\psi \in \{g, h\}$ is

$$\Omega_{\psi_\alpha} = + \frac{1}{\lambda} (\psi_\alpha - \psi_\alpha^{\text{eq}}) \quad (9)$$

$$F_{g_\alpha} = + (e_{\alpha i} - u_i) \left[\partial_i \rho c_s^2 (\Gamma_\alpha(\mathbf{u}) - \Gamma_\alpha(0)) \right. \quad (10)$$

$$\left. + \mu (\partial_i C) \Gamma_\alpha(\mathbf{u}) \right]$$

$$F_{h_\alpha} = + (e_{\alpha i} - u_i) \left[\partial_i C - \frac{C}{\rho c_s^2} (\partial_i p - \mu \partial_i C) \right] \Gamma_\alpha(\mathbf{u}) \quad (11)$$

$$+ M(\partial_k \partial_k \mu) \Gamma_\alpha(\mathbf{u})$$

Here $e_{\alpha i}$ denote the discrete particle velocities in directions α of the velocity lattice and the current work employs the D3Q19 lattice. The relaxation parameter λ is proportional to the kinematic viscosity ν , $\nu = \eta/\rho =$

$c_s^2 \lambda = c_s^2 \tau \delta t$, where we use the definition $\tau \equiv \lambda/\delta t$. It is taken as the harmonic mean of the bulk relaxation parameters (τ_l, τ_v) weighted by C [6],

$$\frac{1}{\tau} = \frac{C}{\tau_l} + \frac{1-C}{\tau_v}. \quad (12)$$

The equilibrium distribution functions g_α^{eq} and h_α^{eq} of Eqs. (7)-(8) are

$$g_\alpha^{\text{eq}} = w_\alpha \left[p + \rho c_s^2 \left(\frac{e_{\alpha i} u_i}{c_s^2} + \frac{(e_{\alpha i} e_{\alpha j} - c_s^2 \delta_{ij}) u_i u_j}{2c_s^4} \right) \right] \quad (13)$$

$$h_\alpha^{\text{eq}} = w_\alpha C \left[1 + \frac{e_{\alpha i} u_i}{c_s^2} + \frac{(e_{\alpha i} e_{\alpha j} - c_s^2 \delta_{ij}) u_i u_j}{2c_s^4} \right] \quad (14)$$

$$\equiv \Gamma_\alpha(\mathbf{u}) C \quad (15)$$

where w_α are the integral weighting factors of the D3Q19 model. Using the Chapman-Enskog expansion, Eqs. (7)-(8) can be shown to recover Eqs. (1) and (5)-(6) to second-order accuracy at low Mach numbers. The hydrodynamic fields are calculated by taking the zeroth and the first moments of the distribution functions [6]

$$C = \sum_\alpha h_\alpha \quad (16)$$

$$\rho u_i = \frac{1}{c_s^2} \sum_\alpha e_{\alpha i} g_\alpha \quad (17)$$

$$p = \sum_\alpha g_\alpha \quad (18)$$

B. Boundary Conditions

Incorporating contact angles can be accomplished by adding to the free energy functional Ψ_b a surface term Ψ_s which accounts for the interaction between the liquid-vapor interface and solid surface. Expanded as a power series in the composition calculated at the solid surface, C_s , the surface term takes the form [31]

$$\Psi_s = \int_S (\phi_0 - \phi_1 C_s + \phi_2 C_s^2 - \phi_3 C_s^3) dS, \quad (19)$$

where terms up to cubic order are retained. The constants ϕ_i for $i \in \{1, 2, 3\}$ are given by $\phi_0 = \phi_1 = 0$, $\phi_2 = \phi_c/2$ and $\phi_3 = \phi_c/3$, where ϕ_c is a constant that recovers the desired contact angle [5-7]. In the linear and quadratic approximations the liquid phase at the solid surface is enriched relative to the bulk value by the attraction on wetting surfaces and depleted due to the repulsion on non-wetting surfaces [5]. This effect is undesirable in the systems that the current work is directed towards, and the cubic approximation is thus utilized which displays equilibrium densities at the solid surface that are equal to the corresponding bulk values.

The first boundary condition required for Eq. (1) ensures no mass flux normal to a solid boundary due to a

chemical potential gradient [6, 7],

$$\mathbf{n} \cdot \nabla \mu|_S = 0, \quad (20)$$

and is satisfied when bounce-back is employed at the solid boundary. The second boundary condition is for $\nabla^2 C$ and can be established by minimizing Ψ_s [5],

$$\mathbf{n} \cdot \nabla C|_S = \frac{\phi_c}{\kappa} (C_s - C_s^2), \quad (21)$$

where the equilibrium contact angle θ_{eq} follows from Young's equation for a given wetting potential Ω_c $\cos \theta_{\text{eq}} = -\Omega_c = -\phi_c / \sqrt{2\kappa\beta}$. Alternative formulations of this boundary condition exist such as the geometric formulation presented in [32].

Simulating wetting effects with the lattice Boltzmann method thus reduces to implicitly imposing Eq. (21) at the solid boundary in the relevant terms of the intermolecular forces. On regular grids this is accomplished by specifying the terms in the finite-difference derivatives at the solid boundary, see *e.g.*, [5–7, 21]. In the following we describe a method for enforcing them on an irregular grid.

C. Finite Element Method

Equations (7)-(8) can be solved at any point by streaming along characteristics from (\mathbf{x}, t) to $(\mathbf{x} + \delta t \mathbf{e}_\alpha, t + \delta t)$ (where δt is the time step), and applying the trapezoid rule to the RHS [21, 26, 30].

$$\begin{aligned} \psi_\alpha(\mathbf{x} + \delta t \mathbf{e}_\alpha, t + \delta t) - \psi_\alpha(\mathbf{x}, t) = \\ \frac{\delta t}{2} (F_{\psi_\alpha} - \Omega_{\psi_\alpha})|_{(\mathbf{x}, t)} + \frac{\delta t}{2} (F_{\psi_\alpha} - \Omega_{\psi_\alpha})|_{(\mathbf{x} + \delta t \mathbf{e}_\alpha, t + \delta t)}. \end{aligned} \quad (22)$$

By introducing the new variable $\bar{\psi}_\alpha(\mathbf{x}, t) = \psi_\alpha + \frac{\delta t}{2} \Omega_{\psi_\alpha}$ we can recast Eq. (22) as

$$\begin{aligned} \bar{\psi}_\alpha(\mathbf{x} + \delta t \mathbf{e}_\alpha, t + \delta t) - \bar{\psi}_\alpha(\mathbf{x}, t) = \\ - \frac{1}{\tau + 0.5} (\bar{\psi}_\alpha - \bar{\psi}_\alpha^{\text{eq}}) + \frac{\delta t}{2} (F_{\psi_\alpha}|_{(\mathbf{x}, t)} + F_{\psi_\alpha}|_{(\mathbf{x} + \delta t \mathbf{e}_\alpha, t + \delta t)}) \end{aligned} \quad (23)$$

where $\bar{\psi}_\alpha^{\text{eq}} = \psi_\alpha^{\text{eq}}$, $\tau = \lambda / \delta t$, and the moments of $\bar{\psi}$ recover the same macroscopic fields as the moments of ψ . The force term can be treated in an implicit manner and integrated locally in the collision step [30]. It is observed, however, that integrating the force term in the streaming step as done in [29] greatly enhances stability when simulating surface wettability, and allows to minimize spurious currents through careful selection of the spatial discretization scheme (as discussed in greater detail below).

Equation (23) is solved at a grid point \mathbf{x}_i using the standard two-step procedure:

Collision

$$\hat{\psi}_\alpha^n = \bar{\psi}_\alpha^n - \frac{1}{\tau + 0.5} (\bar{\psi}_\alpha^n - \bar{\psi}_\alpha^{\text{eq}, n}) \quad (24)$$

Streaming

$$\begin{aligned} \bar{\psi}_\alpha^{n+1} = \hat{\psi}_\alpha^n - \delta t (e_{\alpha i} \partial_i \hat{\psi}_\alpha^n - F_{\psi_\alpha}^n) \\ + \frac{\delta t^2}{2} e_{\alpha j} \partial_j (e_{\alpha i} \partial_i \hat{\psi}_\alpha^n - F_{\psi_\alpha}^n) \end{aligned} \quad (25)$$

where the superscripts correspond to the time step. Equation (25) is obtained from (23) by approximating

$$\begin{aligned} \hat{\psi}^n(\mathbf{x}_i - \delta t \mathbf{e}_\alpha) = \hat{\psi}^n(\mathbf{x}_i) - \delta t e_{\alpha i} \partial_i \hat{\psi}_\alpha^n \\ + \frac{\delta t^2}{2} e_{\alpha j} e_{\alpha i} \partial_j \partial_i \hat{\psi}_\alpha^n + \mathcal{O}(\delta t^3), \end{aligned} \quad (26)$$

$$F_{\psi_\alpha}^n(\mathbf{x}_i - \delta t \mathbf{e}_\alpha) = F_{\psi_\alpha}^n(\mathbf{x}_i) - \delta t e_{\alpha i} \partial_i F_{\psi_\alpha}^n + \mathcal{O}(\delta t^2), \quad (27)$$

$$F_{\psi_\alpha}^{n+1}(\mathbf{x}_i) = F_{\psi_\alpha}^n(\mathbf{x}_i) + \mathcal{O}(\delta t). \quad (28)$$

We note that $F_{\psi_\alpha}^{n+1}(\mathbf{x}_i)$ is approximated by $F_{\psi_\alpha}^n(\mathbf{x}_i)$ in order to avoid implicitness. This approximation still yields a second-order accurate and conditionally stable expression in time (see appendix of [33]). Intuitively, the approximation follows from the observation that the macroscopic fields recovered by $\bar{\psi}_\alpha$ change at a much slower rate than the individual populations.

Equation (25) is discretized in space using the Galerkin finite element method, where spatial decomposition using linear, tetrahedral elements has been applied. The particle distribution functions are specified at the mesh nodes (vertices) $\mathbf{x}_1, \mathbf{x}_2, \dots, \mathbf{x}_{N_V}$ and interpolated at other points,

$$\bar{\psi}_\alpha(\mathbf{x}) \approx \bar{\psi}_\alpha^n(\mathbf{x}) = \mathbf{N}^{(1)}(\mathbf{x})^T \boldsymbol{\psi}_\alpha^n, \quad (29)$$

where $\bar{\psi}_\alpha^n(\mathbf{x})$ is the approximate solution evaluated at a point \mathbf{x} , and $\boldsymbol{\psi}_\alpha^n = [\bar{\psi}_\alpha^n(\mathbf{x}_1), \bar{\psi}_\alpha^n(\mathbf{x}_2), \dots, \bar{\psi}_\alpha^n(\mathbf{x}_{N_V})]^T$ is the vector of the nodal values. Furthermore, $\mathbf{N}^{(1)}(\mathbf{x}) = [\phi_1^{(1)}(\mathbf{x}), \phi_2^{(1)}(\mathbf{x}), \dots, \phi_{N_V}^{(1)}(\mathbf{x})]^T$ where $\phi_i^{(1)}$ is the piecewise-linear shape function corresponding to the node \mathbf{x}_i , satisfying $\phi_i^{(1)}(\mathbf{x}_j) = \delta_{ij}$ by construction.

Special care must be taken when discretizing the force terms in order to reduce spurious currents in the interfacial region and prevent artificial behaviour, such as mass diffusion between phases (and corresponding thickening of the interface). While Wardle and Lee [29] suggest to use the same discretization scheme for the force terms, experiments show that this approach suffers from such unwanted behaviour. An accurate approach can be derived by analysing the numerical method in case of a static interface at equilibrium, in absence of surface tension, *i.e.* $\mathbf{u}(\mathbf{x}) = 0$, $p(\mathbf{x}) = 0$, $\kappa = 0$. In such case $F_{f_\alpha} = w_\alpha e_{\alpha i} \partial_i C$, $F_{g_\alpha} = 0$. Naturally, the collision and streaming equations for g_α preserve zero pressure field. However, when the concentration gradient is non-zero, the streaming term in the equation for f_α results in the diffusion of concentration from the heavier (liquid) phase ($C = 1$) into the lighter (vapor) phase ($C = 0$). This can be balanced out by choosing the discretization of $\tilde{\nabla} C^n$,

such that

$$\sum_{\alpha=0}^K \int_{\Omega_k} \mathbf{e}_\alpha \cdot \left(\nabla \mathbf{N}^{(1)}(\mathbf{x})^T \psi_\alpha^n - \tilde{\nabla} C^n \right) d\Omega = 0, \quad (30)$$

where Ω_k is the k -th element (tetrahedron) in the mesh. In our setting, one such discretization is the piecewise constant one, i.e. $\tilde{\nabla} C^n = \mathbf{N}^{(0)}(\mathbf{x})^T \nabla C^n$, where $\nabla C^n = [\nabla C_1^n, \nabla C_2^n, \dots, \nabla C_{N_T}^n]^T$, ∇C_k^n is the constant concentration gradient inside an element Ω_k , computed from the nodal values of the piecewise linear concentration field $C^n(\mathbf{x}_i) = \sum_{\alpha=0}^K \hat{f}_\alpha^n(\mathbf{x}_i)$, and $\mathbf{N}^{(0)}(\mathbf{x})^T = [\phi_1^{(0)}, \phi_2^{(0)}, \dots, \phi_{N_T}^{(0)}]$, where $\phi_k^{(0)}$ is the piecewise-constant shape function, $\phi_k^{(0)}(\mathbf{x})|_{\Omega_l} \equiv \delta_{kl}$.

The above reasoning suggests to use a piecewise linear discretization for the fields defined through algebraic operations on the distribution functions ψ_α (i.e. C , p , \mathbf{u} , μ and ρ) and a piecewise constant discretization for the force terms F_{ψ_α} : $F_{\psi_\alpha}(\mathbf{x}) = \mathbf{N}^{(0)}(\mathbf{x})^T \Phi_{\psi_\alpha}^n$, where

$$\Phi_{\psi_\alpha}^n = [\Phi_{\psi_\alpha,1}^n, \Phi_{\psi_\alpha,2}^n, \dots, \Phi_{\psi_\alpha,N_T}^n]^T \quad (31)$$

$$\Phi_{\psi_\alpha,k}^n = \frac{1}{|\Omega_k|} \int_{\Omega_k} F_{\psi_\alpha} d\Omega \quad (32)$$

The integral in Eq. (32) above can be approximated with great accuracy within the expected range of values of the hydrodynamic fields by substituting the barycentric values of the piecewise-linear fields into Eqs. (10) and (11). Based on analytical calculations, the largest error within the expected range of physical variables due to this approximation is found to be roughly 1%.

Finally, the weak form of Eq. (25) reads

$$\mathbf{M}^{(1,1)}(\psi_\alpha^{n+1} - \psi_\alpha^n) = \left(-\delta t \mathbf{C}_\alpha - \delta t^2 \mathbf{D}_\alpha \right) \psi_\alpha^n - \left(\delta t \mathbf{M}^{(1,0)} - \delta t^2 \mathbf{K}_\alpha \right) \Phi_{\psi_\alpha}^n \quad (33)$$

where matrices $\mathbf{M}^{(1,1)}, \mathbf{C}_\alpha, \mathbf{D}_\alpha \in \mathbb{R}^{N_V \times N_V}$ and $\mathbf{M}^{(1,0)}, \mathbf{K}_\alpha \in \mathbb{R}^{N_V \times N_T}$ are defined as

$$\mathbf{M}^{(1,1)} = \int_{\mathcal{D}} \mathbf{N}^{(1)} \mathbf{N}^{(1)T} d\Omega \quad (34)$$

$$\mathbf{M}^{(1,0)} = \int_{\mathcal{D}} \mathbf{N}^{(1)} \mathbf{N}^{(0)T} d\Omega \quad (35)$$

$$\mathbf{C}_\alpha = \int_{\mathcal{D}} \mathbf{N}^{(1)} e_{\alpha r} \partial_r \mathbf{N}^{(1)T} d\Omega \quad (36)$$

$$\mathbf{K}_\alpha = \frac{1}{2} \int_{\mathcal{D}} \partial_r \mathbf{N}^{(1)} e_{\alpha r} \mathbf{N}^{(0)T} d\Omega \quad (37)$$

$$\mathbf{D}_\alpha = \frac{1}{2} \int_{\mathcal{D}} \partial_s \mathbf{N}^{(1)} e_{\alpha s} e_{\alpha r} \partial_r \mathbf{N}^{(1)T} d\Omega \quad (38)$$

for the domain \mathcal{D} . The linear system is solved using the preconditioned conjugate gradient method, using the lumped mass vector as the preconditioner.

D. Evaluating Laplacians

The Laplacian terms $\nabla^2 C$ and $\nabla^2 \mu$ in Eqs. (3) and (11), respectively, are stored per element. Looking at the concentration-term first, it is evaluated by considering the volume integral of $\nabla^2 C$ over the set Ω , which contains all elements $\Omega_\alpha, \Omega_\beta, \dots$ that share \mathbf{x}_k as a common vertex

$$\int_{\Omega} \nabla^2 C d\Omega = \int_{\partial\Omega} \nabla C \cdot \mathbf{n} dS, \quad (39)$$

from which we infer

$$\nabla^2 C \approx \frac{1}{\mathcal{V}(\Omega)} \int_{d\Omega} \nabla C \cdot \mathbf{n} dS \quad (40)$$

$$= \frac{1}{\mathcal{V}(\Omega)} \sum_i \int_{e_i} \nabla C \cdot \mathbf{n} dS. \quad (41)$$

The sum in Eq. (41) runs over all outer edges e_i in Ω . For elements where one or more edges e_i are along the solid boundary, the corresponding terms in the integrand in Eq. (41) are substituted by the value in Eq. (21). This is illustrated in Fig. 1 for a two-dimensional system.

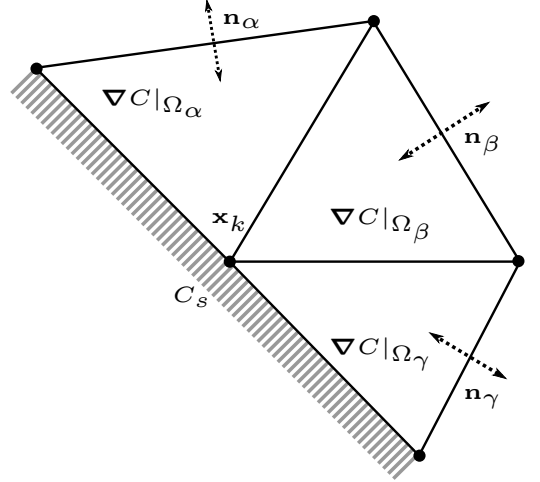


FIG. 1: Triangular finite elements centered at vertex \mathbf{x}_k that form the set $\Omega = \Omega_\alpha \cup \Omega_\beta \cup \Omega_\gamma$ at a solid boundary.

The evaluation of the $\nabla^2 \mu$ -term follows the same reasoning, but the integration is per element Ω_α

$$\nabla^2 \mu \approx \frac{1}{\mathcal{V}(\Omega_\alpha)} \int_{d\Omega_\alpha} \nabla \mu \cdot \mathbf{n} dS \quad (42)$$

$$= \frac{1}{\mathcal{V}(\Omega_\alpha)} \sum_i \int_{e_i} \nabla \mu \cdot \mathbf{n} dS \quad (43)$$

where the integrands along a line segment e_i separating adjacent elements Ω_α and Ω_β are taken as the average and the value at line segments along the solid boundary are taken as zero as per Eq. (20). This is illustrated in Fig. 2.

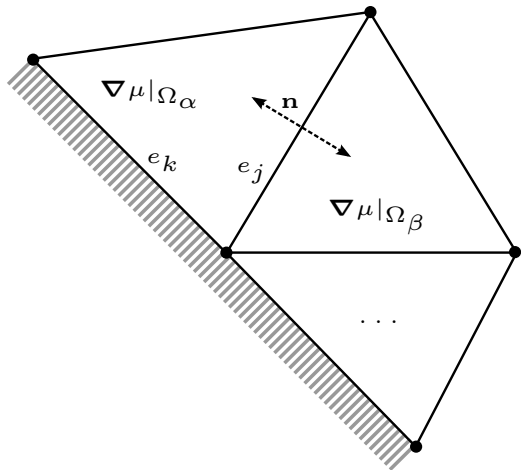


FIG. 2: Triangular finite elements at a solid boundary. The value at the line segment e_j is taken as $\nabla\mu|_{e_j} = 0.5(\nabla\mu|_{\Omega_\alpha} + \nabla\mu|_{\Omega_\beta}) \cdot \mathbf{n}$ and $\nabla\mu|_{e_k} = 0$.

III. RESULTS AND DISCUSSION

A. Parasitic Currents

We assess the performance of the scheme by first considering a droplet with radius R in a stationary flow. The average parasitic kinetic energy in the interfacial region $R \pm \xi$ of the droplet is reported in Table I for the mixed scheme described in Section II C alongside values obtained using the nodal discretization presented in our earlier work [30]. The mixed discretization scheme is observed to successfully decrease the parasitic currents by two orders of magnitude compared to the nodal discretization. As outlined in Subsection II D this reduction is due to the piecewise constant (linear) discretization of the force terms (physical fields) that balance out the diffusion of concentration from the liquid phase to the vapor phase.

Elements	$\langle \rho \mathbf{u} \cdot \mathbf{u} \rangle_N$	$\langle \rho \mathbf{u} \cdot \mathbf{u} \rangle_M$
$1.5 \cdot 10^6$	$0.95 \cdot 10^{-6}$	$3.16 \cdot 10^{-9}$
$2.9 \cdot 10^6$	$0.14 \cdot 10^{-6}$	$1.61 \cdot 10^{-9}$
$4.9 \cdot 10^6$	$0.048 \cdot 10^{-6}$	$0.65 \cdot 10^{-9}$

TABLE I: Average parasitic kinetic energy density $\langle \rho \mathbf{u} \cdot \mathbf{u} \rangle$ in the region $R \pm \xi$ of a static droplet using the nodal (N) and mixed (M) scheme on different mesh resolutions. The two phases have a density contrast of $\rho_l/\rho_g = 2$ and identical kinematic viscosities.

B. Contact Angle Measurements

We now turn to an investigation of the equilibrium shape of a three-dimensional droplet on a homogeneous surface. The droplet is initialized as a perfect hemisphere resting on a plane surface with radius $R = 1$, see Fig. 3. Also illustrated is the underlying unstructured mesh. It is generated with an increasing resolution towards the bottom surface where the interface dynamics occurs, thereby enhancing the accuracy of the simulation without a significant increase in required computation time.

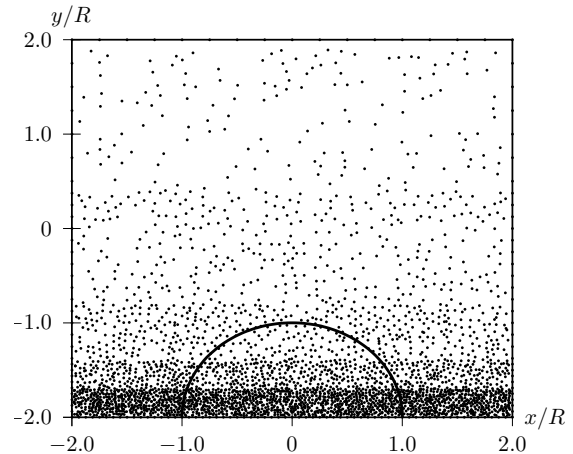


FIG. 3: A cross section of the unstructured grid used for the droplet-simulations. The mesh contains $N = 1.5 \cdot 10^6$ grid points in total. Also shown is the initial contour $C = 0.5$.

In Fig. 4a three equilibrium contours are shown of a droplet with a wetting potential corresponding to $\theta_{\text{eq}} = 150^\circ$. It is assumed that the droplet has reached equilibrium when the kinetic energy converges to a steady value asymptotically. The contact angle is then measured from the droplet height h and base diameter b as $\theta = \pi - \arctan(b/2(r - h))$, where $r = (4h^2 + b^2)/8h$. Although the interface is several lattice units thick, the measurements are performed on the contour $C = 0.5$.

In Fig. 4b the full range of angles has been simulated by varying the wetting potential Ω_c for two set of density- and kinematic viscosity ratios $\{M_\rho, M_\nu\}$ and fixed surface tension $\sigma = 0.0025$. In general, we obtain good results for moderate contact angles. The largest discrepancy (23°) appears for a fully non-wet surface. For $45 \lesssim \theta_{\text{eq}} \lesssim 135$ the simulated angle is within 5° of the theoretical value. It has been explicitly verified that these results are independent of the mesh resolution and interface width.

The time evolution of the kinetic energy per unit volume for $\theta_{\text{eq}} = 120^\circ$ is shown in Fig. 5 for different values of the mobility. Following [7, 34], the effect of mobility is characterized by the dimensionless number $S = \sqrt{M\rho_l\nu_l}/R$. It is observed that the spurious cur-

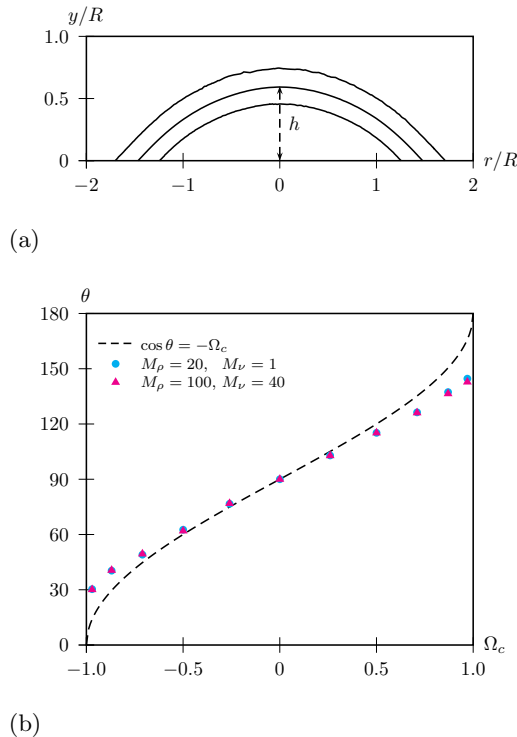


FIG. 4: (a) Cross sections of the equilibrium contours ($C = 0.1$, $C = 0.5$ and $C = 0.9$) for a droplet with $\theta_{\text{eq}} = 150^\circ$ and contrasts $M_\rho = 100$ and $M_\nu = 40$. (b) Measured equilibrium contact angle θ as a function of dimensionless wetting potential Ω_c .

rents decay at a faster rate for larger values of S , *i.e.*, larger values of mobility.

C. Capillary Intrusion

We now consider the injection of a wetting liquid through a cylindrical capillary tube in order to assess whether the present FE-LBM is able to simulate correct displacement behavior and capture the capillary effect. Following the classical analysis by Washburn [35], we neglect the viscosity of the vapor phase, gravity and inertial effects and furthermore assume that the intruding liquid is incompressible and obeys Poiseuille flow. The average flow velocity of three-dimensional Poiseuille flow is given by

$$\langle v \rangle = -\frac{(H/2)^2}{8\eta_l} \frac{dp}{dx}, \quad (44)$$

where H denotes the pipe diameter, η_l the liquid dynamic viscosity and dp/dx the pressure gradient that drives the liquid. The Laplace drop across a curved interface is $\Delta p = 2\sigma/R$, where σ is the surface tension between the two phases and R the radius of curvature of the interface. The gradient is then $dp/dx = -2\sigma/(Rl)$, where l is the

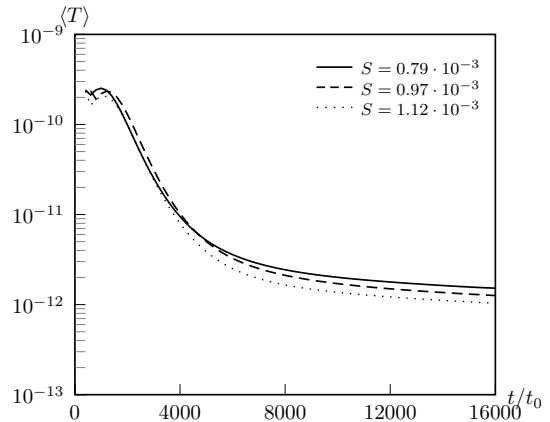


FIG. 5: Time evolution of the average kinetic energy density in lattice units $\langle T \rangle = 0.5 \sum_i (\rho_i \mathbf{u}_i \cdot \mathbf{u}_i)/N$ for a droplet with $M_\rho = 100$, $M_\nu = 40$ and fixed contact angle $\theta_{\text{eq}} = 120^\circ$. The mobility M is varied through $S = \sqrt{M} \rho_l \nu_l / R$. Time is scaled by the viscous time $t_0 = \rho_l \nu_l R / \sigma$.

length of the liquid that has penetrated the capillary. The relation between R and the curvature (wetting) angle θ is $R = H/(2 \cos \theta)$. By substituting these relations in Eq. (44) and using $\langle v \rangle = dy/dt$, we obtain the following equation of motion for the interface movement

$$\frac{dy}{dt} = \frac{H\sigma \cos \theta}{8\eta_l}. \quad (45)$$

The simulation setup is illustrated in Fig. 6a. The mesh contains roughly 10^6 elements and is periodic along the symmetry axis (y) of the capillary. The middle portion of length $L = 20H$ has no-slip wetting boundaries and the boundary conditions are periodic in all directions outside of the middle portion. Fig. 6b presents the results of our simulations of hydrophilic capillaries with contact angles $\theta = 83^\circ$, $\theta = 72^\circ$ and $\theta = 56^\circ$. The results display good agreement with theory.

IV. CONCLUSION

In this study a new implementation of the FE-LBM has been developed for simulating liquid droplet behaviour on partial wetting surfaces at large density and kinematic viscosity ratios. The scheme is based on the free-energy multiphase model of Wardle and Lee [6, 29] and augments our previous nodal-based FE-LBM formulation [30] by discretizing the intermolecular forces at elements. Furthermore, the integration of the forces is now performed in the streaming step.

We have benchmarked our implementation by investigating a liquid droplet in three different settings: Immersed in a vapor phase, resting on a solid surface and

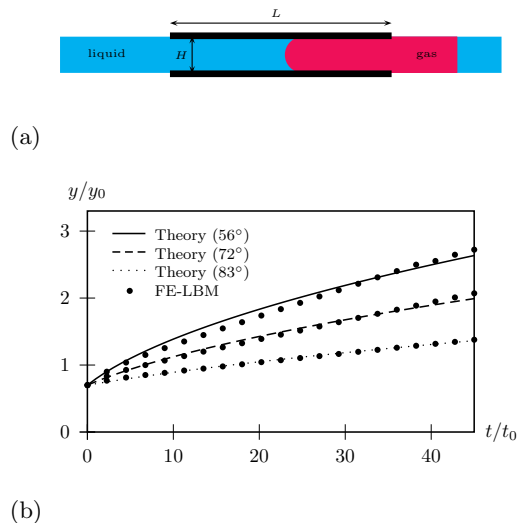


FIG. 6: (a) Simulation setup for capillary intrusion. (b) The length y/y_0 of the column of the intruding liquid as a function of time t/t_0 . Units are scaled by the characteristic length $y_0 = H$ and time $t_0 = H\eta_l/\sigma$.

moving in a capillary due to capillary pressure. The study reveals that the implementation reduces spurious currents at the interface by two orders of magnitude relative to the nodal implementation in [30]. Furthermore, the obtained equilibrium contact angles of the liquid droplet on a solid surface agree within $\pm 5^\circ$ with the angles theoretically predicted by Young's law for partially wetting fluids ($45 \lesssim \theta_{\text{eq}} \lesssim 135$).

In summary, the numerical results indicate that the present FE-LBM scheme is numerically stable and accurate and can be used to study multiphase flows where wetting effects are non-negligible, while harvesting the geometric flexibility of off-lattice schemes. Of particular interest is the effects of reservoir wettability on the relative permeabilities, which is of great importance in reservoir modelling.

V. ACKNOWLEDGMENTS

The authors acknowledge valuable discussions with Taehun Lee. This work is financed by Innovation Fund Denmark and Maersk Oil and Gas A/S through the P³ project.

-
- [1] A. Briant, *Philosophical Transactions of the Royal Society of London A: Mathematical, Physical and Engineering Sciences* **360**, 485 (2002).
- [2] A. J. Briant, A. J. Wagner, and J. M. Yeomans, *Phys. Rev. E* **69**, 031602 (2004).
- [3] A. J. Briant and J. M. Yeomans, *Phys. Rev. E* **69**, 031603 (2004).
- [4] T. Lee and L. Liu, *Phys. Rev. E* **78**, 017702 (2008).
- [5] L. Liu and T. Lee, *International Journal of Modern Physics C* **20**, 1749 (2009).
- [6] T. Lee and L. Liu, *Journal of Computational Physics* **229**, 8045 (2010).
- [7] K. Connington and T. Lee, *Journal of Computational Physics* **250**, 601 (2013).
- [8] H. Huang, D. T. Thorne, M. G. Schaap, and M. C. Sukop, *Phys. Rev. E* **76**, 066701 (2007).
- [9] S. Schmieschek and J. Harting, *Communications in Computational Physics* **9**, 11651178 (2011).
- [10] H. P. Jansen, K. Sotthewes, J. van Swigchem, H. J. W. Zandvliet, and E. S. Kooij, *Phys. Rev. E* **88**, 013008 (2013).
- [11] S. Son, L. Chen, D. Derome, and J. Carmeliet, *Computers & Fluids* **117**, 42 (2015).
- [12] L. Wang, H.-b. Huang, and X.-Y. Lu, *Phys. Rev. E* **87**, 013301 (2013).
- [13] H. Liu, A. J. Valocchi, Q. Kang, and C. Werth, *Transport in Porous Media* **99**, 555 (2013).
- [14] A. Ghassemi and A. Pak, *Journal of Petroleum Science and Engineering* **77**, 135 (2011).
- [15] A. G. Yiotis, J. Psihogios, M. E. Kainourgiakis, A. Papaioannou, and A. K. Stubos, *Colloids and Surfaces A: Physicochemical and Engineering Aspects* **300**, 35 (2007).
- [16] K. Langaas and P. Papatzacos, *Transport in Porous Media* **45**, 241 (2001).
- [17] H. Huang and X. yun Lu, *Physics of Fluids* **21**, 092104 (2009).
- [18] H. Huang, Z. Li, S. Liu, and X.-y. Lu, *International Journal for Numerical Methods in Fluids* **61**, 341 (2009).
- [19] H. Liu, Q. Kang, C. Leonardi, S. Schmieschek, A. Narvez, B. Jones, J. Williams, A. Valocchi, and J. Harting, *Computational Geosciences*, 1 (2015).
- [20] H. Huang, C. M. Sukop, and X.-Y. Lu, *Multiphase Lattice Boltzmann Methods: Theory and Application*, 1st ed. (Wiley, 2015).
- [21] K. W. Connington, T. Lee, and J. F. Morris, *Journal of Computational Physics* **283**, 453 (2015).
- [22] N. Rossi, S. Ubertini, G. Bella, and S. Succi, *International Journal for Numerical Methods in Fluids* **49**, 619 (2005).
- [23] D. V. Patil and K. Lakshmisha, *Journal of Computational Physics* **228**, 5262 (2009).
- [24] M. K. Misztal, A. Hernandez-Garcia, R. Matin, H. O. Sørensen, and J. Mathiesen, *Journal of Computational Physics* **297**, 316 (2015).
- [25] T. Lee and C.-L. Lin, *Journal of Computational Physics* **171**, 336 (2001).
- [26] T. Lee and C.-L. Lin, *Journal of Computational Physics* **185**, 445 (2003).
- [27] A. Bardow, I. V. Karlin, and A. A. Gusev, *Europhysics Letters* **75**, 434 (2006).
- [28] M. K. Misztal, A. Hernandez-Garcia, R. Matin, D. Müter, D. Jha, H. O. Sørensen, and J. Mathiesen, *Frontiers in Physics* **3** (2015), 10.3389/fphy.2015.00050.
- [29] K. E. Wardle and T. Lee, *Computers and Mathematics with Applications* **65**, 230 (2013), special Issue on Mesoscopic Methods in Engineering and Science (ICMMES-2010, Edmonton, Canada).
- [30] R. Matin, M. K. Misztal, A. Hernandez-Garcia, and J. Mathiesen, *Computers & Mathematics with Applications* **74**, 281 (2017).
- [31] P. G. de Gennes, *Rev. Mod. Phys.* **57**, 827 (1985).
- [32] H. Ding and P. D. M. Spelt, *Phys. Rev. E* **75**, 046708 (2007).
- [33] T. Lee, C.-L. Lin, and L.-D. Chen, *Journal of Computational Physics* **215** (2006), 10.1016/j.jcp.2005.10.021.
- [34] P. YUE, C. ZHOU, and J. J. FENG, *Journal of Fluid Mechanics* **645**, 279294 (2010).
- [35] E. W. Washburn, *Phys. Rev.* **17**, 273 (1921).